REPORT DOCUMENTATION PAGE

Form Approved OMB NO. 0704-0188

1. REPORT DATE (DD-MM-YYYY)	2. REPORT TYPE	3. DATES COVERED (From - To)
12-10-2018	Final Report	1-Jun-2014 - 30-Nov-2017

4. TITLE AND SUBTITLE

Final Report: Design of Thermal Metamaterials Beyond the Effective Medium Theory: Direct Numerical Simulation via the Thermal Discrete Dipole Approximation (T-DDA)

5a. CONTRACT NUMBER
W911NF-14-1-0210

5b. GRANT NUMBER

5c. PROGRAM ELEMENT NUMBER
611102

6. AUTHORS

5d. PROJECT NUMBER

5e. TASK NUMBER

5f. WORK UNIT NUMBER

7. PERFORMING ORGANIZATION NAMES AND ADDRESSES

University of Utah
75 South 2000 East

Salt Lake City, UT 84112 -8930

8. PERFORMING ORGANIZATION REPORT NUMBER

9. SPONSORING/MONITORING AGENCY NAME(S) AND ADDRESS (ES)

U.S. Army Research Office
P.O. Box 12211
Research Triangle Park, NC 27709-2211

10. SPONSOR/MONITOR'S ACRONYM(S)
ARO

11. SPONSOR/MONITOR'S REPORT NUMBER(S)
64546-MS-YIP.26

12. DISTRIBUTION AVAILIBILITY STATEMENT

Approved for public release; distribution is unlimited.

13. SUPPLEMENTARY NOTES

The views, opinions and/or findings contained in this report are those of the author(s) and should not contrued as an official Department of the Army position, policy or decision, unless so designated by other documentation.

14. ABSTRACT

15. SUBJECT TERMS

16. SECURITY CLASSIFICATION OF:			17. LIMITATION OF ABSTRACT	15. NUMBER OF PAGES	19a. NAME OF RESPONSIBLE PERSON
a. REPORT	b. ABSTRACT	c. THIS PAGE			Mathieu Francoeur
UU	UU	UU	UU		19b. TELEPHONE NUMBER
					801-581-5721

RPPR Final Report
as of 31-Oct-2018

Agency Code:

Proposal Number: 64546MSYIP **Agreement Number: W911NF-14-1-0210**
INVESTIGATOR(S):

Name: Mathieu Francoeur
Email: mfrancoeur@mech.utah.edu
Phone Number: 8015815721
Principal: Y

Organization: **University of Utah**
Address: 75 South 2000 East, Salt Lake City, UT 841128930
Country: USA

DUNS Number: 009095365 EIN: 876000525
Report Date: 28-Feb-2018 Date Received: 12-Oct-2018
Final Report for Period Beginning 01-Jun-2014 and Ending 30-Nov-2017
Title: Design of Thermal Metamaterials Beyond the Effective Medium Theory: Direct Numerical Simulation via the Thermal Discrete Dipole Approximation (T-DDA)
Begin Performance Period: 01-Jun-2014 **End Performance Period:** 30-Nov-2017
Report Term: 0-Other

Submitted By: Mathieu Francoeur Email: mfrancoeur@mech.utah.edu
Phone: (801) 581-5721

Distribution Statement: 1-Approved for public release; distribution is unlimited.

STEM Degrees: 2 **STEM Participants:** 2

Major Goals: The objective of this project was to establish a computational framework for solving near-field thermal radiation problems in three-dimensional (3D) complex geometries. The computational framework developed, implemented, and tested in this project is called the thermal discrete dipole approximation (T-DDA). The T-DDA is based on fluctuational electrodynamics, where a fluctuating current representing thermal emission is added to Maxwell's equations. The research activities were divided into three main tasks:
(1) Implementation of the T-DDA for modeling near-field radiative heat transfer in 3D complex geometries;
(2) Application of the T-DDA for predicting near-field heat radiative transfer between arbitrarily-shaped objects and near-field thermal emission by metamaterials;
(3) Design of metamaterial thermal spectra maximizing thermophotovoltaic (TPV) energy conversion.
This research provided for the first time a computational framework for calculating near-field radiative heat transfer and near-field thermal emission with complex materials beyond the effective medium theory. The outcome of this project will accelerate the implementation of TPV energy converters via the design, fabrication and testing of metamaterials selectively emitting thermal radiation. In addition, this research will impact other technologies capitalizing on near-field thermal radiation such as infrared cloaking and heat flow regulation via photonic thermal diodes through metamaterial design.

Accomplishments: See PDF document uploaded in the "Upload" section. The PDF attachment provides a comprehensive description of the work done under ARO sponsorship. Specifically, the PDF file provides the following items:

1. Statement of the problem studied

2. Summary of the most important results

3. Details of scientific progress and accomplishments

4. Publications under ARO sponsorship

RPPR Final Report
as of 31-Oct-2018

Training Opportunities: ARO sponsorship contributed to the training of three, highly-qualified graduate students.

- Sheila Edalatpour: Sheila was sponsored by the ARO grant until June 2016. She was the driving force for the development, implementation, and testing of the thermal discrete dipole approximation (T-DDA). Before even graduating with her PhD in June 2016, Sheila was hired by the University of Maine as a tenure-track Assistant Professor of Mechanical Engineering.

- John DeSutter: John worked on metamaterial thermal spectra maximizing thermophotovoltaic output power density and conversion efficiency. John will graduate with a PhD in Mechanical Engineering during the fall 2018 semester.

- Lei Tang: Lei worked on the design of nanostructures for optimizing thermal rectification via photonic thermal diodes. Lei graduated with a MS during the summer 2018, and he is currently a PhD student in the Department of Mechanical Engineering at the University of California, Berkeley.

ARO funding allowed training high qualified students with knowledge and expertise in numerical modeling, near-field thermal radiation, metamaterials large-scale computations, optimization, thermophotovoltaics, and heat flow regulation.

Results Dissemination: The complete list of publications under ARO sponsorship is provided in the Appendix of the PDF document uploaded in the "Upload" section. Beyond the publications listed in the Appendix, the following activities have helped promote near-field thermal radiation and further disseminate results obtained under ARO sponsorship:

- Mathieu Francoeur: Co-Organizer and Co-Chair of the 3rd International Workshop on Nano-Micro Thermal Radiation: Energy, Manufacturing, Materials, and Sensing (NanoRad2017), Korea, June 26-28, 2017.

- Mathieu Francoeur: Guest Editor-in-Chief for the Special Issue of the Journal of Quantitative Spectroscopy and Radiative Transfer on Nano-Micro Thermal Radiation, 2017-2018.

- Mathieu Francoeur: Editorial Board Member, Scientific Reports, Nature Publishing Group, 2017-Present.

- Mathieu Francoeur: Associate Editor, Journal of Quantitative Spectroscopy and Radiative Transfer, Elsevier, 2016-Present.

Honors and Awards: - Best presentation award for John DeSutter: J. DeSutter, M.P. Bernardi, and M. Francoeur, “Design of solar thermophotovoltaic power generators using a genetic algorithm,” 2015 AIChE Annual Meeting, Salt Lake City, Utah, November 8-13, 2015.

Although not directly honors and awards, the PI believes that ARO sponsorship contributed to the following items:

- John DeSutter, Graduate Research Fellowship, University of Utah, 2017.

- Promotion of PI Mathieu Francoeur to the rank of tenured Associate Professor, Department of Mechanical Engineering, University of Utah, 2016.

- Promotion of Sheila Edalatpour to the rank of tenure-track Assistant Professor, Department of Mechanical Engineering, University of Maine, 2016.

- Promotion of Mathieu Francoeur as an Editorial Board Member, Scientific Reports, Nature Publishing Group, 2017-Present.

- Promotion of Mathieu Francoeur as an Associate Editor, Journal of Quantitative Spectroscopy and Radiative Transfer, Elsevier, 2016-Present.

Protocol Activity Status:

Technology Transfer: Nothing to report.

RPPR Final Report
as of 31-Oct-2018

PARTICIPANTS:

Participant Type: PD/PI
Participant: Mathieu Francoeur
Person Months Worked: 2.00 **Funding Support:**
Project Contribution:
International Collaboration:
International Travel:
National Academy Member: N
Other Collaborators:

Participant Type: Faculty
Participant: Sheila Edalatpour
Person Months Worked: 2.00 **Funding Support:**
Project Contribution:
International Collaboration:
International Travel:
National Academy Member: N
Other Collaborators:

Participant Type: Graduate Student (research assistant)
Participant: Lei Tang
Person Months Worked: 6.00 **Funding Support:**
Project Contribution:
International Collaboration:
International Travel:
National Academy Member: N
Other Collaborators:

Participant Type: Graduate Student (research assistant)
Participant: John DeSutter
Person Months Worked: 6.00 **Funding Support:**
Project Contribution:
International Collaboration:
International Travel:
National Academy Member: N
Other Collaborators:

CONFERENCE PAPERS:

Publication Type: Conference Paper or Presentation **Publication Status:** 1-Published
Conference Name: ICHMT International Symposium on Advances in Computational Heat Transfer
Date Received: 12-Aug-2016 Conference Date: 25-May-2015 Date Published:
Conference Location: Piscataway, New Jersey
Paper Title: Computational near-field radiative heat transfer: Convergence analysis of the thermal discrete dipole approximation using the exact solution for two spheres
Authors: S. Edalatpour, M. Cuma, T. Trueax, R. Backman, M. Francoeur
Acknowledged Federal Support: **Y**

RPPR Final Report
as of 31-Oct-2018

Publication Type: Conference Paper or Presentation **Publication Status:** 1-Published
Conference Name: 2015 AIChE Annual Meeting
Date Received: 12-Aug-2016 Conference Date: 11-Aug-2015 Date Published: 11-Aug-2015
Conference Location: Salt Lake City, Utah
Paper Title: Design of solar thermophotovoltaic power generators using a genetic algorithm
Authors: J. DeSutter, M.P. Bernardi, M. Francoeur
Acknowledged Federal Support: **Y**

Publication Type: Conference Paper or Presentation **Publication Status:** 1-Published
Conference Name: Electromagnetic and Light Scattering Conference ELS-XVI
Date Received: 29-Aug-2017 Conference Date: 19-Mar-2017 Date Published: 19-Mar-2017
Conference Location: University of Maryland, College Park
Paper Title: Near-field radiation heat transfer between arbitrarily-shaped objects and a surface
Authors: Sheila Edalatpour, Mathieu Francoeur
Acknowledged Federal Support: **Y**

DISSERTATIONS:

Publication Type: Thesis or Dissertation
Institution: Department of Mechanical Engineering, University of Utah
Date Received: 12-Aug-2016 Completion Date: 8/1/16 4:24PM
Title: Numerical modeling of near-field thermal radiation in complex, three-dimensional and multi scale geometries
Authors: Sheila Edalatpour
Acknowledged Federal Support: **Y**

Publication Type: Thesis or Dissertation
Institution: University of Utah
Date Received: 10-Oct-2018 Completion Date: 12/1/18 2:50PM
Title: Investigation of near-field radiation-mediated photonic thermal diodes: From theory to experiment
Authors: Tang, Lei
Acknowledged Federal Support: **Y**

Final Progress Report (FPR)

Dates Covered: 06/01/2014 – 11/30/2017

Mathieu Francoeur, Associate Professor

Department of Mechanical Engineering, University of Utah, Salt Lake City, UT 84112

Proposal Number: 64546-MS-YIP

Agreement Number: W911NF-14-1-0210

Program Manager: Dr. John T. Prater

Title of the Project:

Design of thermal metamaterials beyond the effective medium theory: Direct numerical simulation via the Thermal Discrete Dipole Approximation (T-DDA)

PI:

Mathieu Francoeur, Associate Professor

1495 E 100 S, 1563 MEK

Department of Mechanical Engineering, University of Utah

Salt Lake City, UT 84112

Telephone: 801-581-5721

Fax: 801-581-9826

Email: mfrancoeur@mech.utah.edu

Sponsored Research Office Contact Information:

Tanecia Echols, Sponsored Projects Officer

Office of Sponsored Projects, University of Utah

1471 E Federal Way

Salt Lake City, UT 84102

Phone: 801-585-5443

Fax: 801-581-3007

Email: tanecia.echols@osp.utah.edu

FOREWORD

This Final Progress Report provides a comprehensive summary of the work accomplished under Contract Number W911NF-14-1-0210. Following the statement of the problem studied (section I) and the summary of the most important results (section II), the report describes in detail the fundamentals of the thermal discrete dipole approximation (T-DDA) developed, implemented, and tested during the period covered by this grant. Afterwards, specific results obtained with the T-DDA are discussed. The complete list of publications produced under ARO sponsorship is provided in the Appendix for convenience.

TABLE OF CONTENTS

LIST OF APPENDIXES, FIGURES AND TABLES

I. STATEMENT OF THE PROBLEM STUDIED

The objective of this project was to establish a computational framework for solving near-field thermal radiation problems in three-dimensional (3D) complex geometries. The computational framework developed, implemented, and tested in this project is called the thermal discrete dipole approximation (T-DDA). The T-DDA is based on fluctuational electrodynamics, where a fluctuating current representing thermal emission is added to Maxwell's equations. The research activities were divided into three main tasks:

(1) Implementation of the T-DDA for modeling near-field radiative heat transfer in 3D complex geometries;

(2) Application of the T-DDA for predicting near-field heat radiative transfer between arbitrarily-shaped materials and near-field thermal emission by metamaterials;

(3) Design of thermal emission spectra (i.e., metamaterials) maximizing thermophotovoltaic (TPV) energy conversion.

This research provided for the first time a computational framework for calculating near-field radiative heat transfer and near-field thermal emission with complex materials beyond the effective medium theory. The outcome of this project will accelerate the implementation of TPV energy converters via the design, fabrication and testing of metamaterials selectively emitting thermal radiation. In addition, this research will impact other technologies capitalizing on near-field thermal radiation such as infrared cloaking and heat flow regulation via photonic thermal diodes through metamaterial design.

II. SUMMARY OF THE MOST IMPORTANT RESULTS

The accomplishments are broadly summarized in the next three paragraphs, corresponding to the three tasks of the project listed in section I. Details of the accomplishments and main results are provided in section III.

In Task 1, a novel computational method called the thermal discrete dipole approximation (T-DDA) has been developed, implemented, and tested. The T-DDA is based on the fluctuational electrodynamics framework, where the Maxwell equations are augmented by a fluctuating current representing thermal emission (stochastic Maxwell equations). In the T-DDA, objects are discretized into cubical sub-volumes conceptualized as electric point dipoles. Full electromagnetic interactions between the sub-volumes are taken into account via dyadic Green's functions. The accuracy of the T-DDA has been thoroughly investigated via a convergence analysis for the case of two spheres exchanging thermal radiation, a problem for which exact results are available. The convergence analysis showed that the T-DDA can accurately model near-field thermal radiation problems, and can thus be safely applied to 3D complex geometries and materials (e.g., metamaterials).

In Task 2, the T-DDA has been applied to predicting near-field radiative heat transfer between complex-shaped bodies for which no analytical solution exists. In particular, the case of a probe interacting with a surface has been studied in the context of spectroscopic analysis of near-field thermal emission (i.e., near-field thermal spectroscopy). The T-DDA allowed answering a long-standing question in near-field thermal spectroscopy related to spectral redshift of resonance of the thermal near field scattered in the far zone. In addition, the T-DDA has been applied to directly calculate thermal emission from structures made of multiple inclusions (i.e., metamaterials). As computational resources associated with the T-DDA substantially increase

with increasing the number of sub-volumes, a periodic formulation of the T-DDA has been designed, implemented, and succesfully tested.

In Task 3, a genetic algorithm has been coupled to a thermophotovoltaic (TPV) energy conversion model for determining metamaterial thermal spectra maximizing TPV performances (i.e., output power density and conversion efficiency). The analysis demonstrated that maximization of TPV performances must be done by accounting for all losses in the cell, namely radiative, electrical, and thermal losses. In addition, metamaterial thermal spectra determined using the coupled genetic algorithm-TPV model are a strong function of the parameter to be maximized (conversion efficiency or output power density) when thermal losses in the cell are taken into account.

III. DETAILS OF SCIENTIFIC PROGRESS AND ACCOMPLISHMENTS

III.A. Description of the thermal discrete dipole approximation (T-DDA)

The key result of this project is the development, implementation, and testing of the thermal discrete dipole approximation (T-DDA). The T-DDA is a numerical method, based on fluctuational electrodynamics, used for solving near-field radiative heat transfer problems in three-dimensional (3D) complex geometries. In this section, a comprehensive description of the T-DDA is provided.

The general problem under consideration is shown in Fig. 1, where radiative heat transfer between objects in vacuum and an infinite surface is to be calculated. The vacuum, the surface, and the objects are referred to as medium 0, 1, and 2, respectively. It is assumed that the objects of arbitrary number, shape, and size occupy a total volume V_2 and are isotropic, linear, and non-magnetic. The surface, of volume V_1 and uniform temperature T_1, is assumed to be isotropic, linear, non-magnetic, and is characterized by a homogeneous dielectric function ε_1 local in space. Illumination by external sources (e.g., laser irradiation, thermal emission by the surroundings) is modeled via an incident electric field $\mathbf{E}^{inc}$. The electric field thermal emitted by the surface into the vacuum of volume V_0 is denoted by $\mathbf{E}^{sur}$.

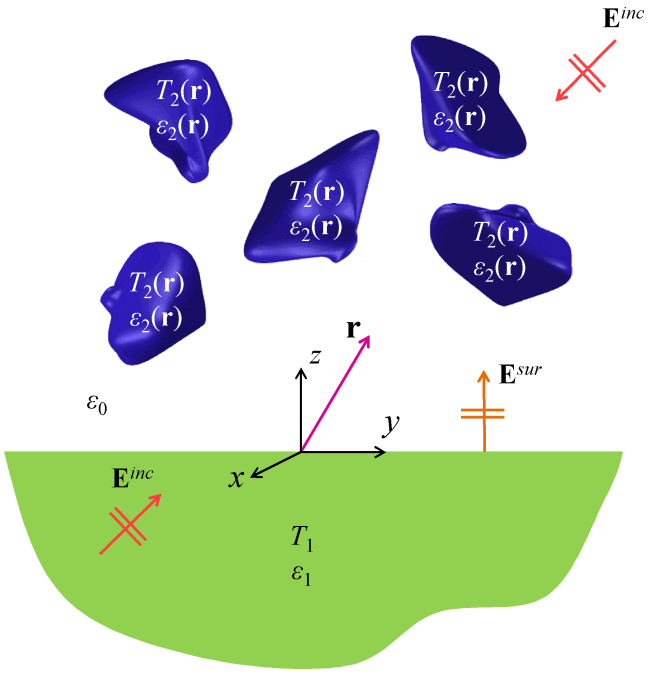

FIG. 1 | Schematic representation of the problem under consideration. Objects (medium 2) are submerged in vacuum (medium 0) above an infinite surface (medium 1). The incident electric field $\mathbf{E}^{inc}$ accounts for illumination by external sources, while the surface field $\mathbf{E}^{sur}$ is the electric field due to thermal emission by the surface.

The net radiative heat rate between the objects and the surface is derived from the stochastic Maxwell equations, where a fluctuating current $\mathbf{J}^{fl}$ is added to Ampère's law:

$$\nabla \times \mathbf{E}(\mathbf{r},\omega) = i\omega\mu_0 \mathbf{H}(\mathbf{r},\omega) \tag{1}$$

$$\nabla \times \mathbf{H}(\mathbf{r},\omega) = -i\omega\varepsilon\varepsilon_0 \mathbf{E}(\mathbf{r},\omega) + \mathbf{J}^{fl}(\mathbf{r},\omega) \tag{2}$$

where $\mathbf{E}$ and $\mathbf{H}$ are the electric and magnetic field intensities, ε is the dielectric function, ε_0 and μ_0 are respectively the permittivity and permeability of vacuum, i is the complex constant, $\mathbf{r}$ is the position vector where the fields are observed, and ω is the angular frequency. The ensemble average of the fluctuating current is zero, while the ensemble average of the spatial correlation

function of the fluctuating current is related to the local temperature of a thermal source via the fluctuation-dissipation theorem [1]:

$$\left\langle \mathbf{J}^{fl}\left(\mathbf{r}',\omega\right)\otimes\mathbf{J}^{fl}\left(\mathbf{r}'',\omega'\right)\right\rangle = \frac{4\omega\varepsilon_0\varepsilon''}{\pi}\Theta\left(\omega,T\right)\delta\left(\mathbf{r}'-\mathbf{r}''\right)\delta\left(\omega-\omega'\right)\overline{\overline{\mathbf{I}}} \tag{3}$$

where $\otimes$ denotes the outer product, $\overline{\overline{\mathbf{I}}}$ is the unit dyadic, ε'' is the imaginary part of the dielectric function of the thermal source and $\Theta(\omega,T)$ is the mean energy of an electromagnetic state given by $\Theta(\omega,T)=\hbar\omega/[\exp(\hbar\omega/k_BT)-1]$.

The electric field everywhere above the surface satisfies the following vector wave equation derived from the stochastic Maxwell equations:

$$\nabla\times\nabla\times\mathbf{E}(\mathbf{r},\omega)-k_0^2\mathbf{E}(\mathbf{r},\omega)=i\omega\mu_0\mathbf{J}(\mathbf{r},\omega),\qquad \mathbf{r}\in V_0\cup V_2 \tag{4}$$

where k_0 is the magnitude of the wavevector in vacuum. The current $\mathbf{J}$ in Eq. (4) is an equivalent source function generating fluctuating and scattered electric fields:

$$\mathbf{J}(\mathbf{r},\omega)=\mathbf{J}_2^{fl}(\mathbf{r},\omega)-i\omega\varepsilon_0\left[\varepsilon_2(\mathbf{r})-1\right]\mathbf{E}(\mathbf{r},\omega),\qquad \mathbf{r}\in V_2 \tag{5}$$

where the subscript 2 in $\mathbf{J}_2^{fl}$ specifies that the fluctuating current is in V_2.

The solution of the inhomogeneous linear differential Eq. (4) is the sum of the solution of the homogeneous equation and a particular solution of the inhomogeneous equation. The homogeneous vector wave equation is given by:

$$\nabla\times\nabla\times\left[\mathbf{E}^{inc}(\mathbf{r},\omega)+\mathbf{E}^{sur}(\mathbf{r},\omega)\right]-k_0^2\left[\mathbf{E}^{inc}(\mathbf{r},\omega)+\mathbf{E}^{sur}(\mathbf{r},\omega)\right]=\mathbf{0},\qquad \mathbf{r}\in V_0\cup V_2 \tag{6}$$

The solution of Eq. (6) provides the electric field that would exist above the surface in the absence of objects. This electric field is comprised of two components, namely the incident field $\mathbf{E}^{inc}$ and the surface field $\mathbf{E}^{sur}$. The surface field is generated by fluctuating currents in V_1, $\mathbf{J}_1^{fl}$, and its expression is given by:

$$\mathbf{E}^{sur}(\mathbf{r},\omega) = i\omega\mu_0 \int_{V_1} \overline{\overline{\mathbf{G}}}^{T}(\mathbf{r},\mathbf{r}',\omega)\cdot\mathbf{J}_1^{fl}(\mathbf{r}',\omega)d^3\mathbf{r}', \qquad \mathbf{r}\in V_0\cup V_2 \tag{7}$$

where $\overline{\overline{\mathbf{G}}}^{T}$ is the transmission dyadic Green's function (DGF) relating the field observed at $\mathbf{r}$ in $V_0\cup V_2$ to a source point $\mathbf{r}'$ located in V_1 [2]. The expression for the incident field satisfies Eq. (6) and depends on the specific external radiation source.

The particular solution of Eq. (4) is the sum of the fluctuating and scattered electric fields generated by the current **J**. The fluctuating and scattered fields are obtained using DGFs relating the electric field observed at **r** to a source located at $\mathbf{r}'$, as shown in Fig. 2, when both **r** and $\mathbf{r}'$ are located above the surface in $V_0\cup V_2$:

$$\mathbf{E}^{sca}(\mathbf{r},\omega)+\mathbf{E}^{fl}(\mathbf{r},\omega) = i\omega\mu_0 \int_{V_2} \overline{\overline{\mathbf{G}}}(\mathbf{r},\mathbf{r}',\omega)\cdot\mathbf{J}(\mathbf{r}',\omega)d^3\mathbf{r}', \qquad \mathbf{r}\in V_0\cup V_2 \tag{8}$$

The DGF $\overline{\overline{\mathbf{G}}}$ is comprised of two components. The first component is the free space DGF, $\overline{\overline{\mathbf{G}}}^{0}$, that accounts for the electric field generated at **r** due to direct radiation by the source **J** located at $\mathbf{r}'$ in the absence of the surface. The second component is the reflection DGF, $\overline{\overline{\mathbf{G}}}^{R}$, representing the electric field generated at **r** due to radiation by the source **J** located at $\mathbf{r}'$ after reflection by the surface.

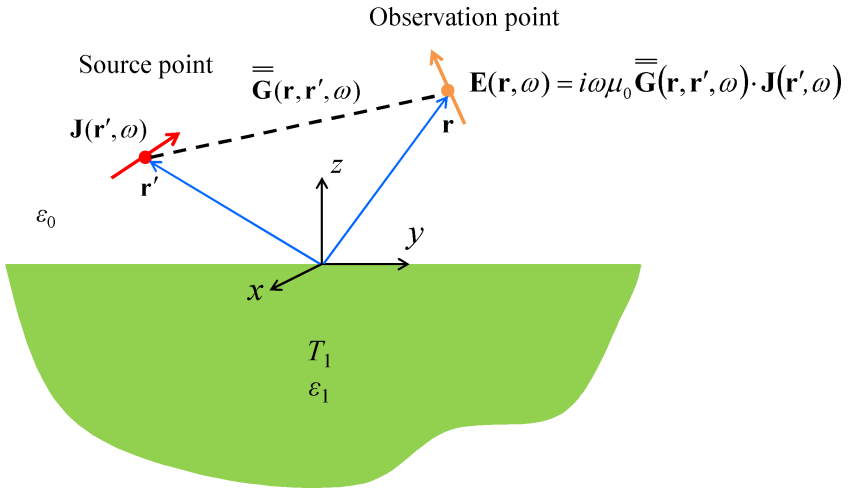

FIG. 2 | Dyadic Green's function (DGF) relating the electric field at $\mathbf{r}$ to a source located at $\mathbf{r}'$ in the presence of a surface.

The volume integral equation for the total electric field in $V_0 \cup V_2$ is obtained by adding the incident and surface fields to Eq. (8):

$$\mathbf{E}(\mathbf{r},\omega)=i\omega\mu_0\int_{V_2}\left(\overline{\overline{\mathbf{G}}}^{0}(\mathbf{r},\mathbf{r}',\omega)+\overline{\overline{\mathbf{G}}}^{R}(\mathbf{r},\mathbf{r}',\omega)\right)\cdot\mathbf{J}(\mathbf{r}',\omega)d^3\mathbf{r}' + \mathbf{E}^{inc}(\mathbf{r},\omega)+\mathbf{E}^{sur}(\mathbf{r},\omega), \qquad \mathbf{r}\in V_0\cup V_2 \tag{9}$$

Solution of Eq. (9) provides the electric field in V_2 from which heat transfer can be calculated. The T-DDA is based on solving Eq. (9) derived from the stochastic Maxwell equations.

The T-DDA formulation is initiated by discretizing V_2 into N cubical sub-volumes. The size of the sub-volumes must be smaller than all characteristic lengths of the problem, namely the wavelength in V_2 and vacuum as well as the object-object and object-surface separation distances. In addition, the sub-volume size must be small enough to represent accurately the object shape via a cubical lattice. When these conditions are fulfilled, the electric field, the DGFs and the electromagnetic properties can be assumed uniform inside a given sub-volume. Under the approximation of uniform electric field, it is possible to conceptualize the sub-volumes as

electric point dipoles. The total dipole moment associated with a sub-volume i of volume ΔV_i is related to the equivalent current via $\mathbf{p}_i = (i/\omega)\int_{\Delta V_i} \mathbf{J}(\mathbf{r}',\omega) d^3\mathbf{r}'$. The discretized volume integral equation for the electric field (9) is written in terms of dipole moments as follows:

$$\frac{1}{\alpha_i}\mathbf{p}_i - \frac{k_0^2}{\varepsilon_0}\sum_{j\neq i}\overline{\overline{\mathbf{G}}}_{ij}^{=0}\cdot\mathbf{p}_j - \frac{k_0^2}{\varepsilon_0}\sum_{j}\overline{\overline{\mathbf{G}}}_{ij}^{=R}\cdot\mathbf{p}_j = \frac{3}{(\varepsilon_{2,i}+2)}\frac{1}{\alpha_i^{CM}}\mathbf{p}_i^{fl} + \mathbf{E}_i^{inc} + \mathbf{E}_i^{sur} \tag{10}$$

where the DGFs $\overline{\overline{\mathbf{G}}}_{ij}^{=0}$ and $\overline{\overline{\mathbf{G}}}_{ij}^{=R}$ are evaluated between the center points of sub-volumes i and j. The total dipole moment $\mathbf{p}_i$ is the sum of two contributions, namely an induced dipole moment $\mathbf{p}_i^{ind} = \Delta V_i \varepsilon_0 (\varepsilon_{2,i} - 1)\mathbf{E}_i$ and a thermally fluctuating dipole moment $\mathbf{p}_i^{fl} = (i/\omega)\int_{\Delta V_i} \mathbf{J}_2^{fl}(\mathbf{r}',\omega) d^3\mathbf{r}'$. Using this last expression in combination with the fluctuation-dissipation theorem (3), the ensemble average of the spatial correlation function of fluctuating dipole moments can be expressed in terms of the local temperature of the medium [3]. The terms α_i^{CM} and α_i are respectively the Clausius-Mossotti and radiative polarizabilities given by:

$$\alpha_i^{CM} = 3\varepsilon_0 \Delta V_i \frac{\varepsilon_{2,i} - 1}{\varepsilon_{2,i} + 2} \tag{11}$$

$$\alpha_i = \frac{\alpha_i^{CM}}{1 - (\alpha_i^{CM}/2\pi\varepsilon_0 a_i^3)[e^{ik_0 a_i}(1 - ik_0 a_i) - 1]} \tag{12}$$

where a_i is the radius of a sphere of volume ΔV_i. The application of Eq. (10) to all N sub-volumes in V_2 results in a system of equations that can be written in a compact matrix form as follows:

$$\left(\overline{\overline{\mathbf{A}}} + \overline{\overline{\mathbf{R}}}\right)\cdot\overline{\mathbf{P}} = \overline{\mathbf{E}}^{fdt} + \overline{\mathbf{E}}^{inc} + \overline{\mathbf{E}}^{sur} \tag{13}$$

where $\overline{\mathbf{E}}^{fdt}$ and $\overline{\mathbf{E}}^{sur}$ are 3N stochastic column vectors containing the first term on the right-hand side of Eq. (10) and the surface field, respectively, while $\overline{\mathbf{E}}^{inc}$ is the 3N deterministic column vector containing the incident field. The term $\overline{\mathbf{P}}$ is the 3N stochastic column vector containing the unknown total dipole moments of the sub-volumes. The matrix $\overline{\overline{\mathbf{A}}}$ is the 3N by 3N deterministic interaction matrix which is composed of sub-matrices $\overline{\overline{\mathbf{A}}}_{ij}$ representing the direct interaction between sub-volumes i and j in the absence of the surface. For brevity, the content of the sub-matrices $\overline{\overline{\mathbf{A}}}_{ij}$ is not provided here and can be found in Ref. [4]. The term $\overline{\overline{\mathbf{R}}}$ is the 3N by 3N deterministic reflection-interaction matrix that contains sub-matrices $\overline{\overline{\mathbf{R}}}_{ij}$ representing the interaction between sub-volumes i and j due to reflection by the surface. For brevity, the content of the sub-matrices $\overline{\overline{\mathbf{R}}}_{ij}$ is not provided here and can be found in Ref. [4].

The net spectral heat rate between the surface and the objects is defined as $\left\langle Q_{net,\omega} \right\rangle = \sum_i \left\langle Q_{abs,\omega,1i} \right\rangle - \sum_i \left\langle Q_{abs,\omega,i1} \right\rangle$, where $\left\langle Q_{abs,\omega,1i} \right\rangle$ is the spectral power absorbed by subvolume i due to thermal emission by the surface and vice-versa for $\left\langle Q_{abs,\omega,i1} \right\rangle$, while $\langle\ \rangle$ denotes a time average. Using reciprocity, the net spectral heat rate can be expressed solely in terms of $\left\langle Q_{abs,\omega,1i} \right\rangle$:

$$\left\langle Q_{net,\omega} \right\rangle = \sum_i \left\langle Q_{abs,\omega,1i} \right\rangle \left[\frac{\Theta\left(\omega, T_{2i}\right)}{\Theta\left(\omega, T_1\right)} - 1 \right] \tag{14}$$

where T_{2i} is the temperature of sub-volume i. The power absorbed $\left\langle Q_{abs,\omega,1i} \right\rangle$ is calculated from the induced dipole moments as follows:

$$\left\langle Q_{abs,\omega,1i} \right\rangle = \frac{\omega}{2}\left(\mathrm{Im}[(\alpha_i^{-1})^*] - \frac{2}{3}k_0^3 \right) \mathrm{tr}\left\langle \mathbf{p}_i^{ind} \otimes \mathbf{p}_i^{ind} \right\rangle \tag{15}$$

where ergodicity is assumed. Note that when calculating the power absorbed, it is assumed that the objects described by V_2 are non-emitting and purely absorbing (T_{2i} = 0 K). Yet, thermal emission by V_2 is accounted for by capitalizing on reciprocity, as shown by Eq. (14). Therefore, $\mathbf{p}_i^{fl} = \mathbf{0}$ and $\mathbf{p}_i = \mathbf{p}_i^{ind}$ for all sub-volumes contained in V_2. The trace of the autocorrelation function of the induced dipole moments in Eq. (15) is obtained directly from the system of equations (13):

$$\left\langle \overline{\mathbf{P}} \otimes \overline{\mathbf{P}} \right\rangle = (\overline{\overline{\mathbf{A}}} + \overline{\overline{\mathbf{R}}})^{-1} \cdot \left\langle (\overline{\mathbf{E}}^{inc} \otimes \overline{\mathbf{E}}^{inc}) + (\overline{\mathbf{E}}^{sur} \otimes \overline{\mathbf{E}}^{sur}) \right\rangle \cdot \left((\overline{\overline{\mathbf{A}}} + \overline{\overline{\mathbf{R}}})^{-1} \right)^{\dagger} \tag{16}$$

where the superscript † indicates the Hermitian operator defined as the conjugate transpose. For brevity, the ensemble average of the spatial correlation function of the surface fields, $\overline{\mathbf{E}}^{sur} \otimes \overline{\mathbf{E}}^{sur}$, is not provided here and can be found in Ref. [4].

Once the dipole moment correlation matrix is computed with Eq. (16), the power absorbed in sub-volume i, $\left\langle Q_{abs,\omega,1i} \right\rangle$, and the net heat rate between the objects and the surface, $\left\langle Q_{net,\omega} \right\rangle$, are respectively calculated with Eqs. (15) and (14).

The T-DDA formalism only involves numerical approximations. Therefore, the T-DDA can be considered as numerically exact since the results obtained from this method converge to the exact solution in the limit that $N \to \infty$, where N is the number of sub-volumes conceptualized as electric point dipoles.

As a final remark, it is worth mentioning that the T-DDA is a numerical approach entirely developed, implemented, and tested in PI Francoeur's group. The T-DDA has already been adopted by other researchers for computing near-field radiative heat transfer and thermal emission based on the fluctuational electrodynamics framework [5].

III.B. Convergence analysis of the thermal discrete dipole approximation (T-DDA)

The convergence and the accuracy of the T-DDA have been studied for the case of two spheres submerged in vacuum. This choice is motivated by the fact that an analytical solution for near-field radiative heat transfer between two spheres is available in the literature [6]. As such, the convergence analysis has been performed by comparing the spectral thermal conductance obtained with the T-DDA against exact results. All computations have been performed with a hybrid OpenMP-MPI parallel T-DDA FORTRAN code utilizing the SCALAPACK library. A schematic representation of this benchmark problem is shown in Fig. 3.

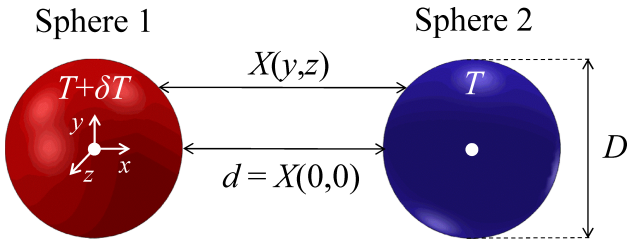

FIG. 3 | Schematic representation of the problem used to analyze the convergence and accuracy of the T-DDA: two spheres of diameter D separated by a distance $X(y,z)$ are exchanging thermal radiation. The minimum distance between the spheres is $d = X(0,0)$.

The spectral thermal conductance is calculated by assuming that sphere 1 is at a temperature $T + \delta T$, while sphere 2 is maintained at a temperature T:

$$G_\omega(T) = \lim_{\delta T \to 0} \frac{\langle Q_{net,\omega} \rangle}{\delta T} \tag{17}$$

where $Q_{net,\omega}$ is the net spectral heat rate between the spheres. The accuracy of the T-DDA has been evaluated for three sizes, $k_0D \ll 1$, $k_0D \approx 1$ and $k_0D \gg 1$. For each size, various gap distances d in the near-field regime of thermal radiation (i.e., $d < \lambda$, where λ is the wavelength in vacuum) have been considered (see Table 1). For each case listed in Table 1, the convergence of the T-DDA has been analyzed for six representative refractive indices (see Table 2), including high and low real and imaginary parts, and a refractive index corresponding to surface phonon-polariton (SPhP) resonance of a silica sphere (refractive index m_f). A total of 42 cases have been investigated, and the results of the convergence analysis are summarized in Table 3.

TABLE 1 | Cases investigated in the convergence analysis.

	k_0D (D)	d/λ (d)
Case 1	0.00628 (10 nm)	0.00100 (10 nm)
Case 2	0.0943 (150 nm)	0.00100 (10 nm)
Case 3	0.0943 (150 nm)	0.0150 (150 nm)
Case 4	1.01 (1.6 μm)	0.00100 (10 nm)
Case 5	1.01 (1.6 μm)	0.100 (1 μm)
Case 6	5.03 (8 μm)	0.0100 (100 nm)
Case 7	5.03 (8 μm)	0.500 (5 μm)

TABLE 2 | Refractive indices investigated in the convergence analysis.

m_a (ε_a)	1.33+0.01i (1.77+0.0266i)
m_b (ε_b)	1.33+1i (0.769+2.66i)
m_c (ε_c)	3+0.01i (9+0.06i)
m_d (ε_d)	3+1i (8+6i)
m_e (ε_e)	3+3i (0+18i)
m_f (ε_f)	0.53+1.28i (-1.36+1.36i)

TABLE 3 | Smallest relative error of the thermal conductance obtained for all cases considered in the convergence analysis (*N*: number of sub-volumes per sphere; *U*: uniform discretization; *NU*: non-uniform discretization).

	Case 1		Case 2		Case 3		Case 4		Case 5		Case 6		Case 7	
	N	Error (%)	N	Error (%)	N	Error (%)	N	Error (%)	N	Error (%)	N	Error (%)	N	Error (%)
m_a	17256 (U)	1.23	29340 (NU)	0.318	17256 (U)	1.22	43324 (NU)	1.01	17256 (U)	1.06	33552 (U)	2.31	33552 (U)	0.115
m_b	17256 (U)	1.79	32572 (NU)	0.572	17256 (U)	1.77	43324 (NU)	3.08	17256 (U)	1.04	48368 (NU)	4.70	33552 (U)	1.68
m_c	36168 (NU)	4.70	33740 (NU)	0.405	19064 (NU)	3.50	43324 (NU)	15.2	17256 (U)	4.14	60200 (NU)	22.1	66796 (NU)	3.83
m_d	49216 (NU)	3.80	23080 (NU)	1.06	19064 (NU)	4.62	43324 (NU)	17.5	39024 (U)	4.45	48368 (NU)	3.03	67472 (NU)	8.33
m_e	59360 (NU)	11.1	59408 (NU)	10.7	74180 (NU)	10.3	77196 (NU)	29.5	72264 (NU)	12.4	81980 (NU)	17.0	70544 (NU)	27.8
m_f	56500 (NU)	4.69	33552 (U)	2.01	35256 (NU)	4.10	43324 (NU)	2.18	52388 (NU)	4.99	33552 (U)	2.75	33552 (U)	0.931

The main conclusions of the convergence analysis are:

a) An error less than 5% was obtained for 74% of the cases studied using up to 82712 sub-volumes per sphere. For all sizes, the accuracy of the T-DDA decreases as both the real and the imaginary parts of the refractive index increase. For all seven cases, the error is maximum for the refractive index m_e having the largest real and imaginary parts ($m_e = 3 + 3i$). However, as shown in Fig. 4 for case 2, there is a converging trend suggesting that the accuracy of the T-DDA is improved by increasing the number of sub-volumes.

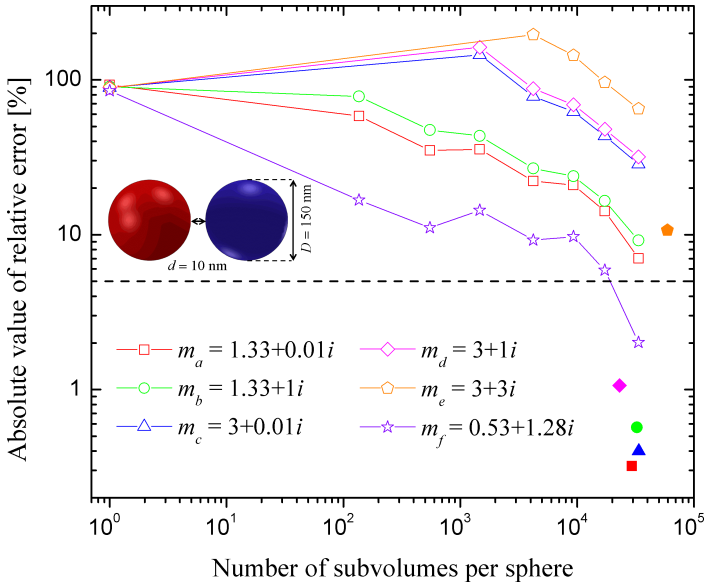

FIG. 4 | Absolute value of the relative error of the thermal conductance as a function of the number of sub-volumes and the refractive index for case 2. Open and filled symbols denote the error for uniform and non-uniform discretizations, respectively.

b) A non-uniform discretization scheme has been implemented (i.e., sub-volumes of different sizes). The results suggest that non-uniform discretization is useful when the sphere to gap ratio, D/d, is large, when $d << \lambda$, and $D < \lambda$, such that significant absorption occurs within a small portion of the sphere (e.g., case 1; see Fig. 5).

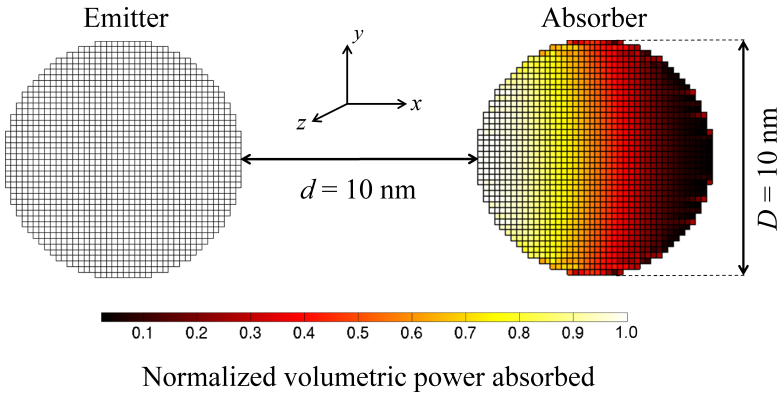

FIG. 5 | Spatial distribution of the normalized volumetric power absorbed for case 1 (refractive index m_c).

c) Fast convergence is achieved when dealing with resonant modes (refractive index m_f). The T-DDA is therefore extremely accurate for predicting SPhP mediated near-field radiative heat transfer. This is important since the total thermal conductance (i.e., conductance integrated over the entire spectrum) is largely dominated by the contribution of SPhP in the near field.

d) The conclusions of the convergence analysis are applicable to geometries other than spheres, except that the error is likely to be smaller due to a weaker shape error. The shape error is the error introduced in the T-DDA formalism when discretizing the objects into cubical sub-volumes.

e) The T-DDA is suitable for objects with sizes smaller than, or of the same order of magnitude as, the wavelength λ. For larger objects, it is not necessary to account for the wave nature of thermal radiation. As such, the classical theory of thermal radiation based on Planck's theory can be used for solving such problems instead of fluctuational electrodynamics.

III.C. Verification of the thermal discrete dipole approximation (T-DDA) with surface interaction

The T-DDA in the presence of a surface, as described in section III.A of this report, has been verified by comparison against the exact solution of heat rate between a 1.6-μm-diameter sphere and a surface [7]. The surface and the sphere are both made of silica and are maintained at temperatures T_1 = 300 K and T_2 = 400 K, respectively. It is assumed that there is no incident electric field. Figure 6 shows the net spectral heat rate obtained from the exact solution and the T-DDA for separation gaps d of 100 nm and 100 μm.

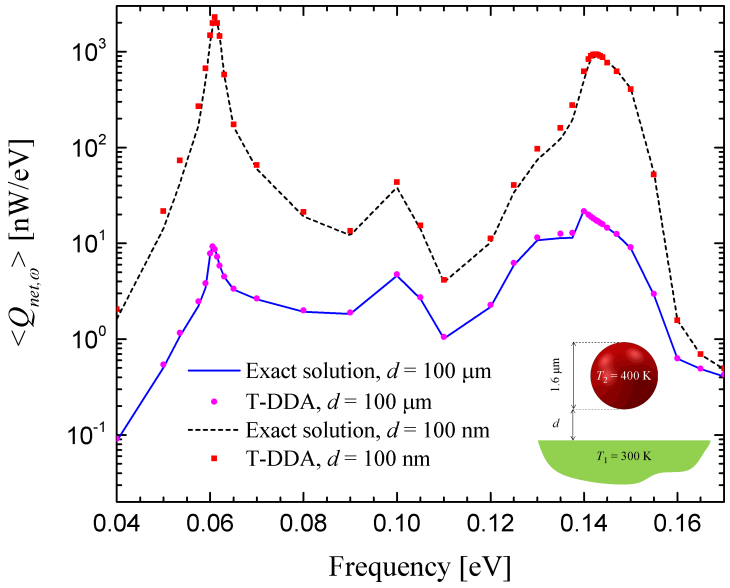

FIG. 6 | Net spectral heat rate between a sphere and a surface for separation gaps d of 100 nm and 100 μm obtained with the T-DDA and the exact solution.

The T-DDA with surface interaction and the exact results are in excellent agreement. The locations of the resonances and their magnitudes are predicted accurately via the T-DDA. The small discrepancy observed for frequencies ranging from 0.1300 eV to 0.1375 eV is due to the fact that the dielectric function of silica is large within that spectral band. A better accuracy could be obtained by employing a larger number of sub-volumes, since the accuracy of the T-DDA increases as the sub-volume size decreases [3]. Yet, increasing the number of sub-volumes within the 0.1300-0.1375 eV spectral band is not necessary as its contribution to the net total heat rate is negligible. The excellent results obtained for the case of a sphere, which is one of the most difficult shapes to model with a cubical lattice, demonstrates that the T-DDA can accurately be used for modeling arbitrarily-shaped objects. As an illustrative example, the T-DDA with surface interaction has been applied for predicting the net spectral heat rate between a complex-shaped probe and a surface, as shown in Fig. 7. Note that exact calculation of near-field radiative heat transfer between a probe and a surface is impossible.

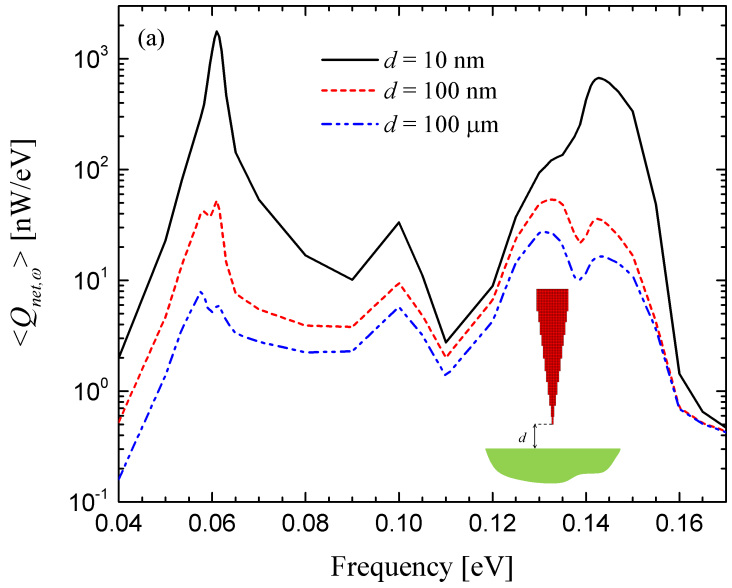

FIG. 7 | Net spectral heat rate between a probe and a surface for separation gaps d of 10 nm, 100 nm and 100 μm.

III.D. Spectroscopic analysis of near-field thermal emission

The T-DDA has been applied to spectroscopic analysis of near-field thermal emission. The ability to probe near-field thermal spectra is of critical importance because several potential applications, such as thermophotovoltaics (TPVs) and thermal rectification, capitalize on spectrally selective near-field radiative exchange via metamaterials. Yet, to date, only a handful of articles have reported spectroscopic measurements of near-field thermal emission by planar heat sources [8-13]. In near-field thermal spectroscopy, the evanescent component of the thermal field is scattered in the far zone using a probing tip brought within a sub-wavelength distance from a heat source. The far-zone scattered field is guided to a Fourier-transform infrared spectrometer, where its spectral distribution is extracted. The collected signal is interpreted as a measurement of the spectral near-field energy density of the heat source. However, all near-field thermal spectroscopy experiments performed with heat sources supporting SPhPs in the infrared (SiC, silicon dioxide, hexagonal boron nitride) have reported resonance redshifts of varying

magnitude, from ~ 5 cm^{-1} to ~ 65 cm^{-1}, using probing tips made of intrinsic Si [9,11], tungsten [10] and platinum-iridium [12]. Using the T-DDA, a critical knowledge gap has been addressed by analyzing the physics of resonance redshift in near-field thermal spectroscopy.

The problem under consideration is shown in Fig. 8(a), where a probe of intrinsic Si couples evanescent modes emitted by a planar heat source of SiC into propagating modes detectable in the far zone. This choice is motivated by the experiments reported in Ref. [11] where spectral redshifts varying from 5 cm^{-1} to 50 cm^{-1} with respect to SPhP resonance of a SiC-vacuum interface were observed on the field scattered by different intrinsic Si probes. In all simulations, the vacuum gap d is fixed at 10 nm, and the surface (T_s) and probe (T_p) temperatures are respectively 573 K and 0 K. Two probe geometries are considered in the simulations (see Fig. 1(b)).

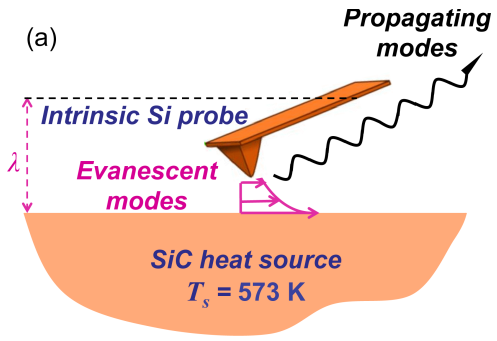

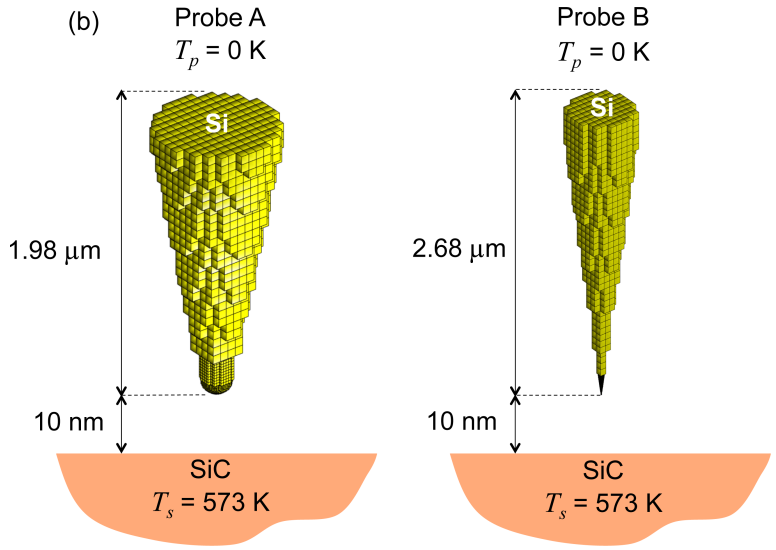

FIG. 8 | (a) Schematic representation of the problem under consideration. The intrinsic Si probe couples evanescent modes emitted by the SiC surface into propagating modes detectable in the far zone. (b) Discretized probes used in T-DDA simulations. Probe A is 1.98-µm-long, has an opening angle of 19°, and a 200-nm-diameter hemispherical tip. Probe B is 2.68-µm-long, has an opening angle of 12°, and a sharp conical tip having a size of 7.2 nm.

The scattered electric field (magnitude squared) in the far zone is obtained from the ensemble average of the induced dipole moments (see Eq. (16)) as follows:

$$\left\langle \left| \mathbf{E}^{\mathrm{FF}}(\mathbf{r}) \right|^2 \right\rangle = \frac{k_0^4}{16\pi^2 r^2} \mathrm{tr}\left(\overline{\overline{\mathbf{F}}} \cdot \left\langle \overline{\mathbf{P}} \otimes \overline{\mathbf{P}} \right\rangle \cdot \overline{\overline{\mathbf{F}}}^{\dagger} \right) \tag{18}$$

In Eq. (18), $\overline{\overline{\mathbf{F}}}$ is the 3 by 3N deterministic matrix accounting for direct emission by the induced dipoles in the far zone (direct component) as well as radiation in the far zone after reflection of dipole emission at the vacuum-SiC interface (indirect component). The matrix $\overline{\overline{\mathbf{F}}}$, obtained using the far-zone approximation of the free space and reflection dyadic Green's functions [14], consists of N 3 by 3 sub-matrices $\mathbf{F}_i$ given by:

$$\mathbf{F}_i = a_i^{\mathrm{TM}} \left(\mathbf{e}_1 \otimes \mathbf{e}_1 \right) + a_i^{\mathrm{TE}} \left(\mathbf{e}_2 \otimes \mathbf{e}_2 \right), \; i = 1,2,\ldots,N \tag{19}$$

In Eq. (19), $\mathbf{e}_1$ and $\mathbf{e}_2$ are unit vectors oriented along the transverse magnetic (TM) and transverse electric (TE) polarizations, respectively, and the coefficient a_i^γ (γ = TM or TE) is defined as:

$$a_i^\gamma = \exp\left(-i\mathbf{k}_{sca}\cdot\mathbf{r}_i\right) + R^\gamma \exp\left(-i\mathbf{k}_{sca}\cdot\mathbf{r}_{\mathrm{I},i}\right) \tag{20}$$

where $\mathbf{r}_i$ is the position vector of sub-volume i, $\mathbf{r}_{\mathrm{I},i}$ is the position vector of the image of sub-volume i with respect to the vacuum-SiC interface, $\mathbf{k}_{sca}$ is the wavevector in the far zone, and R^γ is the Fresnel reflection coefficient for γ-polarized radiation incident from vacuum.

The scattered electric field in the far zone by probes A and B is shown in Fig. 9 at an angle θ of 45° with respect to the surface normal and at a radial distance r of 1 m away from the surface. The near-field thermal energy density in vacuum at a distance Δ of 10 nm above the SiC surface, plotted for comparison, is quasi-monochromatic at a frequency of 948 cm^{-1} (corresponds to SPhP resonance of a SiC-vacuum interface).

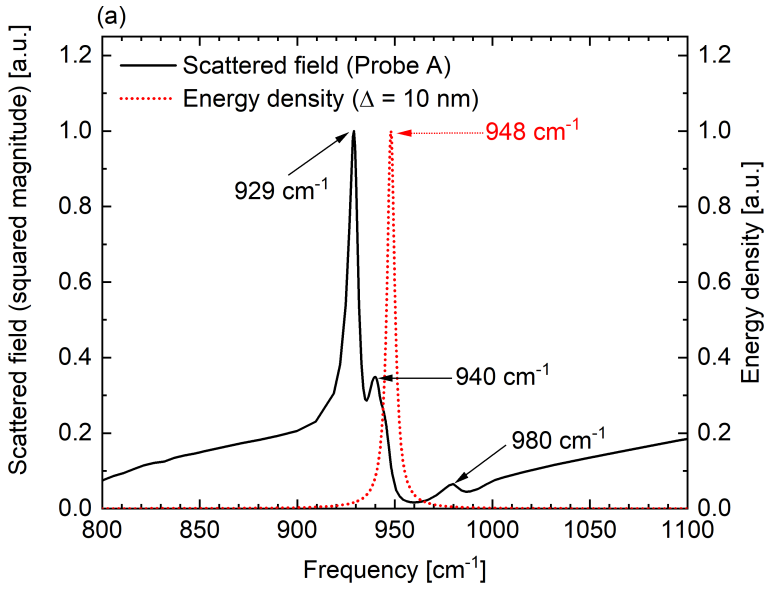

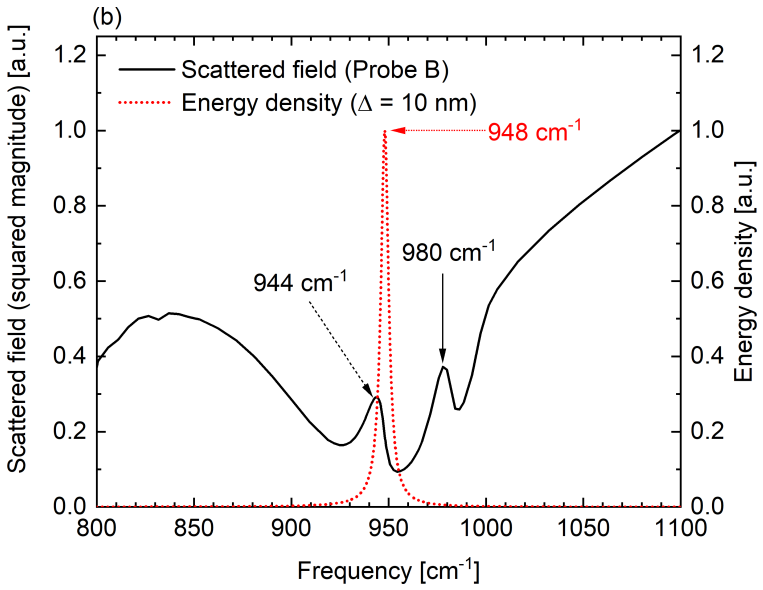

FIG. 9 | Spectral distribution of scattered electric field (magnitude squared) in the far zone at an angle of 45°, with respect to the surface normal, and at a distance of 1 m: (a) Probe A, and (b) Probe B. The spectral distribution of energy density in vacuum in the absence of the probe at a distance of 10 nm with respect to the surface is plotted in both panels for comparison. All curves are normalized by their own maximum.

The spectral distribution of the field scattered by probe A is drastically different from the energy density spectrum. Indeed, the scattered field exhibits a resonance at a frequency of 929 cm^{-1}, which represents a redshift of 19 cm^{-1} with respect to SPhP resonance. A local maximum at a frequency of 940 cm^{-1} is also visible on the scattered field spectrum. The physics underlying SPhP resonance redshift is explained by analyzing gap modes, which are electromagnetic modes existing in the vacuum gap separating the probe and the surface. The eigenfrequencies of gap modes, predicted by Mal'shukov for a lossless sphere-surface configuration under the assumption that that $D >> d$, where D is the sphere diameter, are given by [15]:

$$\frac{1}{\varepsilon_p'(\omega)}+\frac{1}{\varepsilon_s'(\omega)}=-(2m+1)\sqrt{\frac{d}{D}},\ m=0,1,2,... \tag{21}$$

where ε_p' and ε_s' are the real parts of the dielectric function of the surface and the spherical probe, respectively, while m is the order of the gap mode. As probe A is characterized by a 200-nm-diameter hemispherical tip, Eq. (21) is used for predicting gap modes with D = 200 nm. The resulting gap mode eigenfrequencies are 915 cm^{-1}, 942 cm^{-1} and 951 cm^{-1} for the zeroth, first and second order, respectively. Only the zeroth and first order gap modes are visible on the scattered field spectrum, and the predictions made with Eq. (21) are in reasonable agreement with the T-DDA simulations. Conversely, the scattered field spectrum of probe B characterized by a sharp tip with size approximately equal to the vacuum gap thickness d is not greatly impacted by gap modes. As such, a minor redshift of 4 cm^{-1} is observed on the field scattered by probe B.

In summary, the application of the T-DDA to spectroscopic analysis of near-field thermal emission has demonstrated that resonance redshift reported in near-field thermal spectroscopy is mediated by electromagnetic gap modes induced when the probing tip size is much larger than the vacuum gap size. These gap modes affect the scattered field in the far zone even if the probe is non-resonant. The measured signals in near-field thermal spectroscopy experiments should therefore be analyzed using the T-DDA. This analysis has shown unambiguously that the far-zone scattered field cannot be interpreted as a direct measurement of the spectral distribution of near-field thermal energy density.

III.E. Direct calculation of near-field thermal emission by metamaterials

When calculating near-field thermal emission by metamaterials, it is necessary to perform computations for a large number of objects / inclusions. For that purpose, a periodic formulation of the T-DDA has been implemented and verified. This formulation capitalizes on the periodicity of the inclusions in metamaterials. It allows calculating near-field thermal emission by infinite

arrays of inclusions. The idea is to define a single inclusion as the unit cell (UC). The UC is discretized into N cubical sub-volumes behaving as electric point dipoles, as described in section III.A. The UC is on a lattice at location m, n = 0, where m and n are integers along the x- and y-directions, respectively. An infinite number of replicas of the UC along the x- and y-directions are then created (i.e., m, n = -∞ to ∞). Despite the fact that the periodic T-DDA deals with infinite arrays of inclusions, the system of equations is solved only for the N sub-volumes located in the UC, thus keeping the computational cost relatively low.

As a proof-of-concept, a problem involving a one-dimensional (1D) array of nanoparticles, modeled as electric point dipoles, extending to infinity is discussed hereafter (see Fig. 10). A unit cell (UC) is first defined and located on a lattice at m = 0, where m is an integer along the x-direction. The UC in Fig. 10 consists of a single nanoparticle modeled as an electric point dipole (i.e., one sub-volume). In general, the UC may consist of one or more objects discretized into N sub-volumes. The physical location of a given sub-volume i in the UC is denoted by $\mathbf{r}_{i,0}$. An infinite number of replicas of the UC along the x-direction is generated (i.e., m = -∞ to ∞). The physical location of replica m of sub-volume i is given by $\mathbf{r}_{i,m} = \mathbf{r}_{i,0} + m\mathbf{L}_u$, where $\mathbf{L}_u$ is the lattice vector for the array. Assuming that there is no surface and no incident field, the only source of excitation is the fluctuating field. The fluctuating fields in the sub-volumes located in the replicas are phase-shifted with respect to the fluctuating field in sub-volume i of the UC:

$$\mathbf{E}^{fl}(\mathbf{r}_{i,m},\omega) = \mathbf{E}^{fl}(\mathbf{r}_{i,0},\omega)\exp(i\mathbf{k}_0 \cdot m\mathbf{L}_u) \tag{22}$$

As such, the replica dipole moments $\mathbf{p}_{i,m}$ are also phase-shifted relative to the dipole moments $\mathbf{p}_{i,0}$ in the UC:

$$\mathbf{p}_{i,m} = \mathbf{p}_{i,0}\exp(i\mathbf{k}_0 \cdot m\mathbf{L}_u) \tag{23}$$

In that case, the T-DDA equation (10) is modified as follows:

$$\left[\frac{1}{\alpha_i}+\left(\frac{1}{\alpha_i}-\frac{3}{(\varepsilon_i+2)\alpha_i^{CM}}\right)\sum_{m\neq 0}\exp(i\mathbf{k}_0\cdot m\mathbf{L}_u)\right]\mathbf{p}_{i,0}-\frac{k_0^2}{\varepsilon_0}\sum_{j\neq i}\sum_{m\neq 0}\overline{\overline{\mathbf{G}}}^{0}_{ij,m}\cdot\mathbf{p}_{j,0}\exp(i\mathbf{k}_0\cdot m\mathbf{L}_u) = \frac{3}{(\varepsilon_{2,i}+2)}\frac{1}{\alpha_i^{CM}}\mathbf{p}_{i,0}^{fl} \tag{24}$$

Solution of Eq. (24) provides the dipole moment $\mathbf{p}_{i,0}$ in the UC. The dipole moments in the replicas $\mathbf{p}_{i,m}$ are afterwards calculated using Eq. (23).

Figure 10 shows spectral distribution of near-field energy density of a metamaterial made of a 1D infinite array of nanoparticles made of SiC embedded in a lossless medium having a dielectric function of 4. The energy density above a metamaterial is calculated as:

$$\left\langle u_\omega(\mathbf{r})\right\rangle = \frac{\omega^3}{\pi c_0^4}\sum_i\left|\frac{3\alpha_i}{(\varepsilon_i+2)\alpha_i^{CM}}\right|^2\varepsilon_i''\Delta V_i\Theta(\omega,T_i)tr[\overline{\overline{\mathbf{G}}}_{\mathbf{r}i}\otimes\overline{\overline{\mathbf{G}}}_{\mathbf{r}i}] \tag{25}$$

where $\overline{\overline{\mathbf{G}}}_{\mathbf{r}i}$ is the dyadic Green's function of the system (i.e., accounts for the presence of all inclusions) between sub-volume i and the location where the energy density is calculated, $\mathbf{r}$. Results are in perfect agreement with those obtained for a finite chain of 17 nanoparticles. As pointed out by Tervo et al. [16], converged results of energy density are obtained for 17 nanoparticles, which is confirmed by the periodic T-DDA.

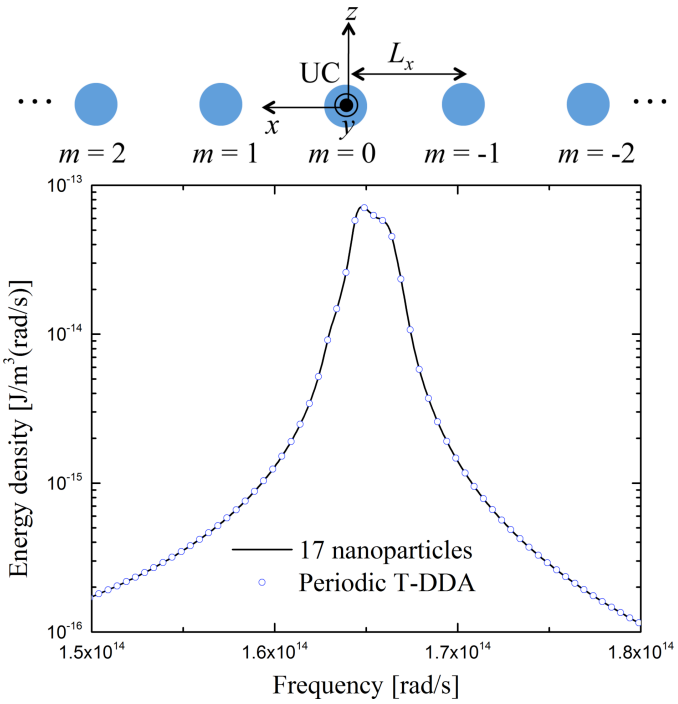

FIG. 10 | Thermal emission by an array of nanoparticles extending to infinity**.** The results are compared against those for 17 nanoparticles. The diameter of the nanoparticles is 50 nm, the distance between the nanoparticles (center-to-center) is fixed at 75 nm, and the distance where the energy density is calculated is 25 nm.

In summary, the results obtained with the periodic formulation show that the T-DDA can be used for direct calculation of near-field thermal emission by metamaterials.

III.F. Determination of metamaterial thermal spectra maximizing thermophotovoltaic (TPV) energy conversion

Metamaterial thermal spectra maximizing TPV energy conversion have been designed. More specifically, the publicly available genetic algorithm (GA) PIKAIA [17] has been coupled to a TPV code developed in PI Francoeur's laboratory [18] in order to determine metamaterial thermal spectra maximizing TPV output power density (P_m) and conversion efficiency (η). Thermal emission spectra maximizing conversion efficiency and output power density are shown in Fig. 11, where the thermal spectrum of a tungsten radiator is also shown for comparison

purpose. In Fig. 12, the performances obtained from the optimal spectra are shown and are compared against the performance obtained with a tungsten and a blackbody radiator. In all cases, radiative, electrical and thermal losses are taken into account in the simulations.

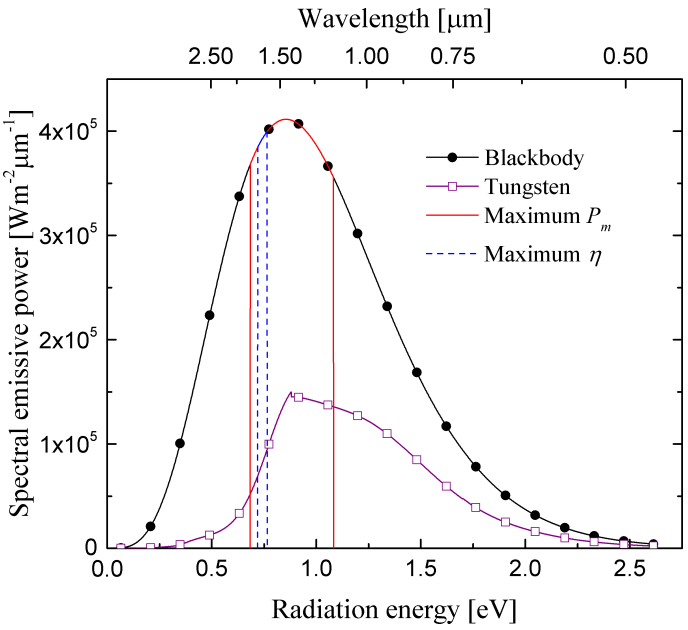

FIG. 11 | Spectral emissive power of various radiators: spectrum maximizing output power density, spectrum maximizing conversion efficiency, blackbody, tungsten.

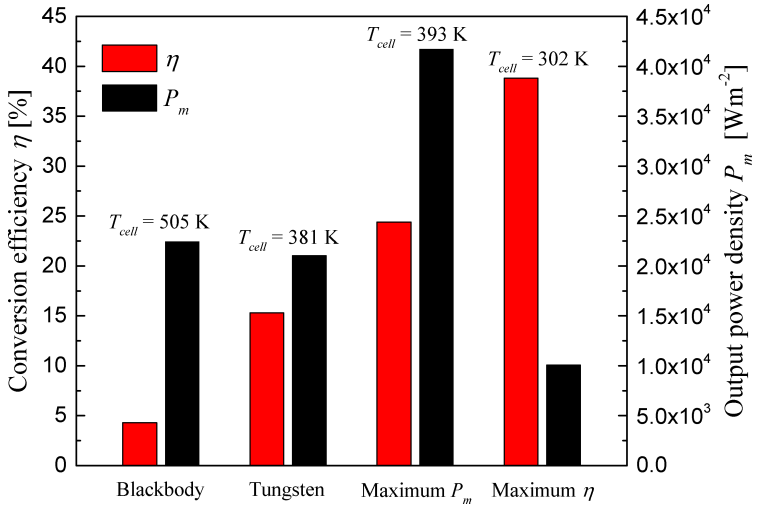

FIG. 12 | Output power density P_m and conversion efficiency η obtained with various radiators: spectrum maximizing output power density, spectrum maximizing conversion efficiency, blackbody, tungsten.

Figure 12 demonstrates that that metamaterial thermal spectra maximizing output power density and conversion efficiency largely outperform blackbody emission and a tungsten radiator commonly used in TPV device. In addition, it can be observed in Fig. 11 that both thermal emission spectra maximizing TPV performance are narrowband (i.e., blackbody emission in a limited spectral band). Such narrowband thermal emission spectra cannot be obtained via naturally occurring materials. This confirms in a rigorous manner one of the hypotheses underlying this research: High-performance power generation via TPV devices can be obtained only via man-made structures (i.e., metamaterials) selectively emitting thermal radiation. Thus, designer materials are necessary for the design, development and implementation of high-performance TPV power generators.

III.G. Design of thermal diodes

Note that although not included in the original proposal, nanostructures and metamaterials can also be used in thermal diodes. A photonic thermal diode is a two-terminal device in which the magnitude of radiative heat flow depends on the direction of the temperature bias. The performance of a thermal diode is typically quantified by the rectification efficiency, defined as $\eta(T_h,T_l) = |Q_f - Q_r|/\max(Q_f,Q_r)$, where Q_f and Q_r are heat rates for the same temperature bias $\Delta T = T_h - T_l$, but in different, forward and reverse, directions. An alternative and simple diode concept leading to high rectification efficiency has been investigated, where both terminals are made of the same material supporting SPhPs in the infrared. Rectification is achieved by switching the terminals on- and off-resonance via the direction of the temperature bias; on- and off-resonance is obtained by capitalizing on the temperature-dependence of coupled SPhPs in nanostructures.

The proposed rectification concept is illustrated via the photonic thermal diode shown in Fig. 13 consisting of two planar structures, called terminals *A* and *B*, separated by a sub-wavelength vacuum gap of thickness *d*. Both terminals are made of 3*C*-SiC, supporting SPhPs in the infrared, but are structurally dissimilar in order to induce on- and off-resonance as a function of the temperature bias direction. Specifically, terminal *A* is made of a SiC thin film coated on a substrate. Unless otherwise mentioned, the substrate is assumed to be lossless (i.e., $\varepsilon_{A2} = \varepsilon'_{A2} + i\varepsilon''_{A2},\ \varepsilon''_{A2} = 0$). Terminal *A* thus support two resonant modes, namely a high-frequency anti-symmetric and a low-frequency symmetric mode, due to SPhP coupling within the thin film. Terminal *B* consists of a bulk (i.e., optically thick) layer of SiC, and therefore supports a single resonant mode. Rectification is achieved by tuning the antisymmetric mode of terminal *A* on- and off-resonance with the mode of terminal *B* as a function of the temperature bias direction. An advantage of using a nanostructure such as a thin film comes from the fact that non-resonant thermal emission of propagating and frustrated modes, detrimental to rectification efficiency, is greatly reduced since it is proportional to the volume of the heat source.

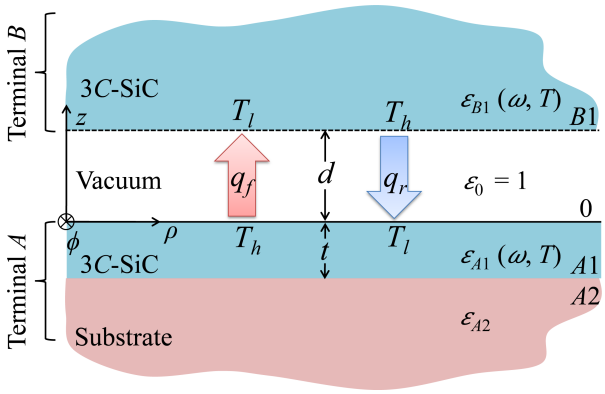

FIG. 13 | Schematic of the photonic thermal diode under consideration, where the terminals are separated by a vacuum gap of size *d*. Terminal *A* is made of a film of 3*C*-SiC with thickness *t* coated on a substrate. Terminal *B* consists of a bulk of 3*C*-SiC.

The key results are summarized in Fig. 14. By analogy with electrical rectification, a current-bias curve (i.e., total heat flux q versus temperature bias ΔT) is plotted for $D = 0.1$, $\varepsilon'_{A2} = 12$ and $d =$ 10 nm in Fig. 14. Clearly, the forward flux is increasing with ΔT at a much faster rate than the reverse flux, since the forward flux tends to be on-resonance while the reverse heat flux is off-resonance as ΔT increases. Starting at a temperature bias of approximately 400 K (i.e., $T_h = 700$ K), a large difference of approximately one order of magnitude between the forward and reverse fluxes is maintained. As such, high rectification efficiency between 80% and 87% is obtained for a wide temperature bias range.

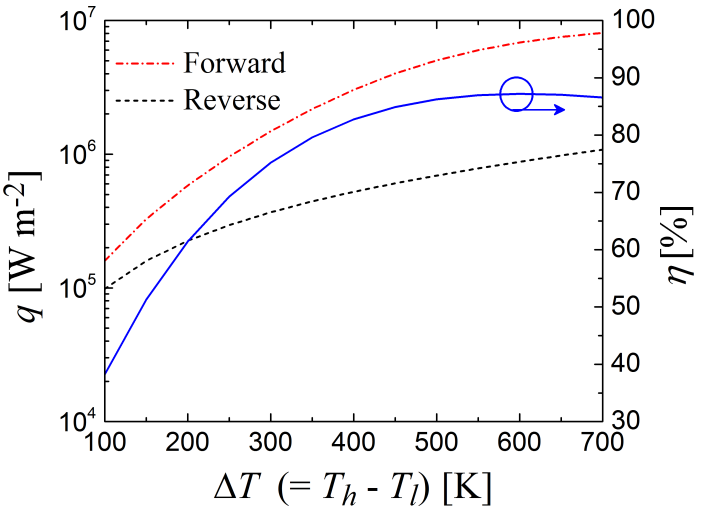

FIG. 14 | Total heat flux q and rectification efficiency η as a function of the temperature bias ΔT (= $T_h - T_l$) for $D =$ 0.1, $\varepsilon'_{A2} = 12$ and $d = 10$ nm.

This work demonstrated that high rectification efficiency can be obtained in a photonic thermal diode with terminals made of the same material supporting SPhPs in the infrared, but with dissimilar structures. It was shown that a specific diode design involving a film and a bulk of 3*C*-SiC can maintain a rectification efficiency in the 80% to 87% range for a wide temperature band (~ 700 K to 1000 K). The upper limit of rectification efficiency can potentially be enhanced by

investigating different nanostructures (e.g., gratings, multilayered media, metamaterials) and other materials supporting SPhPs in the infrared (e.g., silicon dioxide).

IV. BIBLIOGRAPHY

[1] S.M. Rytov, Y.A. Kravtsov, V.I. Tatarskii, *Principles of Statistical Radiophysics 3: Elements of Random Fields*, Springer, New York, 1989.

[2] M. Francoeur, M.P. Mengüç, and R. Vaillon, *Journal of Quantitative Spectroscopy and Radiative Transfer* **110**, 2002-2018, 2009

[3] S. Edalatpour, M. Cuma, T. Trueax, R. Backman, and M. Francoeur, *Physical Review E* **91**, 063307, 2015.

[4] S. Edalatpour and M. Francoeur, *Physical Review B* **94**, 045406, 2016.

[5] R.M. Abraham Ekeroth, A. Garcia-Martin, and J.C. Cuevas, *Physical Review B* **95**, 235428, 2017.

[6] A. Narayanaswamy and G. Chen, *Physical Review B* **77**, 075125, 2008.

[7] C. Otey and S. Fan, *Physical Review B* **84**, 245431, 2011.

[8] Y. De Wilde, F. Formanek, R. Carminati, B. Gralak, P.-A. Lemoine, K. Joulain, J.-P. Mulet, Y. Chen, and J.-J. Greffet, *Nature* **444**, 740, 2006.

[9] A. C. Jones and M. B. Raschke, *Nano Letters* **12**, 1475, 2012.

[10] A. Babuty, K. Joulain, P. O. Chapuis, J. J. Greffet, and Y. De Wilde, *Physical Review Letters* **110**, 1, 2013.

[11] B. T. O'Callahan, W. E. Lewis, A. C. Jones, and M. B. Raschke, *Physical Review B* **89**, 245446, 2014.

[12] B. T. O'Callahan and M. B. Raschke, *APL Photonics* **2**, 21301, 2017.

[13] F. Peragut, L. Cerruti, A. Baranov, J. P. Hugonin, T. Taliercio, Y. De Wilde, and J. J. Greffet, *Optica* **4**, 1409, 2017.

[14] R. Schmehl, B. M. Nebeker, and E. D. Hirleman, *J. Opt. Soc. Am. A* **14**, 3026, 1997.

[15] A. Mal'shukov, *Phys. Rep.* **194**, 343, 1990.

[16] Tervo E., Zhang Z.M. and Cola B., Collective near-field thermal emission from polaritonic nanoparticle arrays, *Physical Review Materials* **1**, 015201, 2017.

[17] PIKAIA: http://www.hao.ucar.edu/modeling/pikaia/pikaia.php. October 11 2018.

[18] M. Francoeur, R. Vaillon, and M.P. Mengüç, *IEEE Transactions on Energy Conversion* **26**, 686-698, 2011.

APPENDIX: PUBLICATIONS UNDER ARO SPONSORSHIP

(a) Papers published in peer-reviewed journals: 7 publications, 1 paper under review.

[1] S. Edalatpour, V. Hatamipour and M. Francoeur, "Spectral redshift of the thermal near field scattered by a probe," *Physical Review Letters*, under review, manuscript available at: https://arxiv.org/abs/1810.02432, 2018.

[2] L. Tang and M. Francoeur, "Photonic thermal diode enabled by surface polariton coupling in nanostructures," *Optics Express* **25**, A1043-A1052, 2017.

[3] S. Edalatpour and M. Francoeur, "Near-field radiative heat transfer between arbitrarily-shaped objects and a surface," *Physical Review B* **94**, 045406, 2016.

[4] S. Edalatpour, J. DeSutter and M. Francoeur, "Near-field thermal electromagnetic transport: An overview," *Journal of Quantitative Spectroscopy and Radiative Transfer* **178**, 14-21, 2016.

[5] J. DeSutter, M. Bernardi, and M. Francoeur, "Determination of thermal emission spectra maximizing thermophotovoltaic performance using a genetic algorithm," *Energy Conversion and Management* **108**, 429-438, 2016.

[6] J.-M. Geffrin, M. Chamtouri, O. Merchiers, H. Tortel, A. Litman, J.-S. Bailly, B. Lacroix, M. Francoeur and R. Vaillon, "The Surface Wave Scattering - Microwave Scanner (SWS-MS)," *Journal of Quantitative Spectroscopy and Radiative Transfer* **168**, 1-9, 2016.

[7] S. Edalatpour, M. Cuma, T. Trueax, R. Backman, and M. Francoeur, "Convergence analysis of the thermal discrete dipole approximation," *Physical Review E* **91**, 063307, 2015.

[8] S. Corbitt, M. Francoeur, and B. Raeymaekers, "Implementation of optical dielectric metamaterials: A Review," *Journal of Quantitative Spectroscopy and Radiative Transfer* **158**, 3-16, 2015.

(b) Papers published in non-peer-reviewed journals: None.

(c) i. Presentations at meetings, but not published in Conference Proceedings: 7 products.

[9] S. Edalatpour and M. Francoeur, "Spectral redshift of the thermal near field scattered by a probe," *2018 MRS Spring Meeting & Exhibit*, Phoenix, Arizona, USA, April 2-6, 2018 (Oral presentation).

[10] S. Edalatpour and M. Francoeur, "Near-field thermal radiation interactions between a probe and a surface," *2nd Thermal and Fluids Engineering Conference and 4th International Workshop on Heat Transfer*, Las Vegas, NV, April 2-5, 2017 (Oral presentation).

[11] J. DeSutter, R. Vaillon, and M. Francoeur, "External luminescence in near-field thermophotovoltaics," *2nd Thermal and Fluids Engineering Conference and 4th International Workshop on Heat Transfer*, Las Vegas, NV, April 2-5, 2017 (Oral presentation).

[12] J. DeSutter, R. Vaillon, and M. Francoeur, "Impacts of near-field radiation on recombination mechanisms in thermophotovoltaics," *ASME 2016 International*

Mechanical Engineering Congress & Exposition, Phoenix, AZ, November 11-17, 2016 (Oral presentation).

[13] S. Edalatpour and M. Francoeur, "Near-field radiation heat transfer between arbitrarily-shaped objects and a surface," *ASME 2016 International Mechanical Engineering Congress & Exposition*, Phoenix, AZ, November 11-17, 2016 (Oral presentation).

[14] S. Edalatpour and M. Francoeur, "The thermal discrete dipole approximation for near-field radiative heat transfer modeling between arbitrarily-shaped objects and a surface," *Thirteenth International Conference on Near-Field Optics, Nanophotonics, and Related Techniques*, Salt Lake City, UT, August 31 - September 4, 2014 (Abstract).

[15] M. Chamtouri, O. Merchiers, M. Francoeur, H. Tortel, J.-M. Geffrin and R. Vaillon, "Electromagnetic surface wave scattering with microwaves," *Progress in Electromagnetics Research Symposium (PIERS) 2014*, Guangzhou, China, August 25-28, 2014 (Extended Abstract).

(c) ii. Non-peer-reviewed conference proceeding publications: 3 products.

[16] S. Edalatpour, M.P. Bernardi, J. DeSutter, and M. Francoeur, "Near-field thermal electromagnetic transport," *Electromagnetic and Light Scattering XV*, Leipzig, Germany, June 21-26, 2015 (Invited presentation).

[17] M. Francoeur, "Near-field radiative heat transfer: Multiscale modeling and measurement between macroscale planar surfaces," *2017 MRS Spring Meeting & Exhibit*, *Symposium NM2 - Nanoscale Heat Transport: From Fundamentals to Devices*, Phoenix, Arizona, USA, April 17-21, 2017 (Invited presentation).

[18] M. Francoeur, "Fluctuational electrodynamics and near-field thermal radiation," *Electromagnetic and Light Scattering XVII*, College Station, Texas, USA, March 4-9, 2018 (Invited presentation).

(c) iii. Peer-reviewed conference proceeding publications: 3 products.

[19] S. Edalatpour and M. Francoeur, "Near-field radiation heat transfer between arbitrarily-shaped objects and a surface," *The 16th Electromagnetic and Light Scattering Conference*, College Park, MD, USA, March 19-25, 2017.

[20] J. DeSutter, M.P. Bernardi, and M. Francoeur, "Design of solar thermophotovoltaic power generators using a genetic algorithm," *2015 AIChE Annual Meeting*, Salt Lake City, Utah, November 8-13, 2015.

[21] S. Edalatpour, M. Cuma, T. Trueax, R. Backman, and M. Francoeur, "Computational near-field radiative heat transfer: Convergence analysis of the thermal discrete dipole approximation using the exact solution for two spheres," *ICHMT International Symposium on Advances in Computational Heat Transfer*, Rutgers University, Piscataway, NJ, May 25 - 29, 2015.

(d) Manuscripts: 1 PhD dissertation and 1 MS thesis.

[22] L. Tang, "Investigation of near-field radiation-mediated photonic thermal diode: From theory to experiment," M.S. Thesis, Department of Mechanical Engineering, University of Utah, Salt Lake City, UT, 2018.

[23] S. Edalatpour, "Numerical modeling of near-field thermal radiation in complex, three-dimensional and multi scale geometries," Ph.D. Dissertation, Department of Mechanical Engineering, University of Utah, Salt Lake City, UT, 2016.

(e) Book and book chapters: 1 book chapter.

[24] M. Francoeur, "Near-Field Thermal Radiation," In: *Handbook of Thermal Science and Engineering*, Springer, 1-43, 2017

(f) Honors and awards: 1 award.

Best presentation award for John DeSutter: J. DeSutter, M.P. Bernardi, and M. Francoeur, "Design of solar thermophotovoltaic power generators using a genetic algorithm," *2015 AlChE Annual Meeting*, Salt Lake City, Utah, November 8-13, 2015.

Although not directly honors and awards, the PI believes that ARO sponsorship contributed to the following items:

- John DeSutter, Graduate Research Fellowship, University of Utah, 2017.
- Promotion of PI Mathieu Francoeur to the rank of tenured Associate Professor, Department of Mechanical Engineering, University of Utah, 2016.
- Promotion of Sheila Edalatpour to the rank of tenure-track Assistant Professor, Department of Mechanical Engineering, University of Maine, 2016.
- Promotion of Mathieu Francoeur as an Editorial Board Member, Scientific Reports, Nature Publishing Group, 2017-Present.
- Promotion of Mathieu Francoeur as an Associate Editor, Journal of Quantitative Spectroscopy and Radiative Transfer, Elsevier, 2016-Present.

(g) Titles of patents disclosed during the reporting period: None.

(h) Patents awarded during the reporting period: None.